Polymer Chemistry

Kinetics and mechanisms of polycondensation reactions between aryl halides and bisphenol A

Journal:	*Polymer Chemistry*
Manuscript ID	PY-ART-05-2020-000740.R1
Article Type:	Paper
Date Submitted by the Author:	02-Jul-2020
Complete List of Authors:	Yang, Yi; Arizona State University Muhic, Christopher; Arizona State University, Chemical Engineering Green, Matthew; Arizona State University, Chemical Engineering

Kinetics and mechanisms of polycondensation reactions between aryl halides and bisphenol A

Yi Yang, Christopher L. Muhich, and Matthew D. Green*

Department of Chemical Engineering; School for Engineering of Matter, Transport and Energy, Arizona State University, Tempe, AZ 85287, USA

Keywords: Polysulfone, Step-growth kinetics, Cation-activated nucleophilic substitution

Abstract: Aryl chlorides (ArCl) or aryl fluorides (ArF) were used in polycondensation reactions to form poly(arylene ether sulfone)s (PAES). Interestingly, the kinetics of the ArF reaction fit a third-order rate law, which is attributed to the activation of the carbon-fluorine bond by two potassium cations (at least one bound to phenolate), which form a three-body complex. The ArCl monomer follows a second-order rate law, where a two-body complex forms at the initial state of the aromatic nucleophilic substitution (S_NAr) pathway. These metal cation-activated complexes act as intermediates during the attack by the nucleophile. This finding was reproduced with either the potassium or the sodium counterion (introduced via potassium carbonate or sodium carbonate). Through a combination of experimental analysis of reaction kinetics and computational calculations with density functional theory (DFT) methods, the present work extends the fundamental understanding of polycondensation mechanisms for two aryl halides and highlights the importance of the CX–metal interaction(s) in the S_NAr reaction, which is translational to other ion-activated substitution reactions.

Introduction

The most widely used synthetic method to produce poly(arylene ether sulfone)s (PAES) for industrial and research purposes[1–12] consists of polycondensation reactions of bisphenols with 4,4'-dichlorodiphenyl sulfone (DCDPS) or with 4,4'-difluorodiphenyl sulfone (DFDPS) in an aprotic polar solvent such as dimethyl sulfoxide (DMSO) using potassium carbonate (K_2CO_3) as the base (**Scheme 1**).[13–15] The reaction typically begins with the deprotonation of bisphenols (pK_a = 9.6 ~ 11.3) by a slight excess of K_2CO_3 (conjugate acid pK_a = 10.25) to produce 1) phenolate compounds, which act as the electron withdrawing group in the subsequent polycondensation reaction with the aryl halide; and 2) side products, including water and carbon dioxide from the further decomposition of the protonated bicarbonate ion under the reaction heat. The mechanism behind this polycondensation reaction is widely accepted as a classical S_NAr, in which the aryl halide is activated toward nucleophilic attack by an electron withdrawing group.[16,17] In aromatic nucleophilic substitution (S_NAr) reactions, the rate limiting step is typically the formation of the resonance-stabilized anionic intermediate, the Meisenheimer complex[18] (**Schemes 2,3**), for which the reactivity of the aryl halide decreases in the order F ≫ Cl>Br>I based on the electronegativity of the halogen.[16] Thus, it is rational to assume that the S_NAr reaction for any aryl dihalide monomer and bisphenol-based nucleophile would follow a second order rate law.[17]

Interestingly, in our present work, the order of the reaction for the aryl fluoride monomer (i.e., DFDPS) was different than that for the aryl chloride monomer (i.e., DCDPS). As expected, the reaction rate of the polymerization using the DFDPS monomer was significantly higher than that of the DCDPS monomer under identical experimental conditions. Ross and coworkers studied the base-catalyzed S_NAr mechanism in the reaction of 1-chloro-2,4-dinitrobenzene and allylamine, which was self-catalyzed by both the amine and aromatic nitro groups.[19–21] They showed that the reaction kinetics fit a third-order rate expression. A computational study[22] related to the synthesis of polysulfones showed that the Meisenheimer complex formed via the formation of a two-body complex with a strong interaction between the metal cation and the aryl fluoride. However, the influence of the monomer interactions with the base on the rate law order in polycondensation reactions of different aryl halides has not been systematically studied using both experimental and computational techniques. In the present work, we systematically compared the kinetics of DFDPS/bisphenol-A (BPA) and DCDPS/BPA reactions during PAES synthesis and revealed surprising insights into the activity of the metal ion and its effect on the reaction kinetics in the two aryl halide systems. While we utilized BPA in order to prepare model PAES macromolecules, we predict that the findings will translate to PAESs prepared using other bisphenol monomers (e.g., 4,4'-biphenol, bisphenol F, etc.). The commercial relevance of polysulfones and the widespread use of S_NAr reactions suggest these findings would be of interest to the greater organic chemistry and polymer science communities.

Experimental Section

Materials and reagents

4,4'-Dichlorodiphenyl sulfone (DCDPS, 98%) was purchased from Sigma-Aldrich and recrystallized from diethyl ether before use. 4,4'-Difluorodiphenyl sulfone (DFDPS, >98%) was purchase from ThermoFisher Scientific Chemical and recrystallized from diethyl ether before use. Bisphenol A (BPA, ≥99%) was purchased from BDH® VMR analytical and recrystallized from acetic acid/water (1:1 v/v) before use. THF and toluene (99.8%) were purchased from Sigma-Aldrich and used after passing through M. Braun SPS-800 solvent purification system. Dimethyl sulfoxide (DMSO, anhydrous, ≥99.9%) was purchased from Sigma-Aldrich and used as received. Potassium carbonate (K_2CO_3, ≥98%) and sodium carbonate (Na_2CO_3, ≥98%) were purchased from Sigma-Aldrich and vacuum dried overnight before use. Deuterated chloroform ($CDCl_3$, 99.8 atom% D, 0.03% (v/v) TMS) was purchased from BDH® VMR analytical and used as received.

Synthesis of poly(arylene ether sulfone)s

The poly(arylene ether sulfone)s (PAES) were synthesized using traditional polycondensation reaction conditions. One reaction protocol for a DCDPS/BPA reaction is provided as an example. It is worth noting that different reaction temperatures and aryl halide monomers (DFDPS vs. DCDPS) were utilized for various studies performed herein (e.g., the stoichiometry study vs. the kinetics study). BPA (1.049 g, 4.605 mmol), DCDPS (1.406 g, 4.899 mmol), K_2CO_3 (0.667 g, 4.835 mmol) were added to a three-neck, 250-mL flask equipped with a condenser, Dean Stark trap, nitrogen inlet/outlet, and a mechanical stirrer. DMSO (24 mL) and toluene (6 mL) were added to the flask to dissolve the monomers. The solution was heated to 140 ˚C and refluxed for 1~6 h to remove the azeotropic mixture of toluene and water using the Dean Stark trap. The reaction continued for 48 h at 140 ˚C. Again, this protocol is provided as an example, the specific reaction temperatures and times utilized are noted in the figures and discussion below for each individual study. After the reaction, the mixture was cooled to room temperature and filtered to remove the precipitated salt. Then the clear solution was diluted with THF, passed through a 0.45 μm Teflon® filter, and precipitated by addition to stirring DI water. The polymer was filtered and dried under vacuum at 100 °C for 24 h. The yields of the final purified polymer products were all more than 95% by weight.

Synthesis of potassium phenolate precursor

The potassium phenolate precursor was prepared by mixing potassium carbonate (1 g, 7.246 mmol) and bisphenol-A (1.652 g, 7.246 mmol) in 50 mL of DI water at 40 ˚C for at least 20 h until the solution became homogeneous. Then the potassium phenolate salt was obtained by evaporating water out of the aqueous solution completely via a rotary evaporator and then vacuum dried at 80 ˚C for 48 h.

Characterizations of polymers and precursor

^{1}H-NMR spectroscopy was performed on a Varian 400 MHz spectrometer using $CDCl_3$ to analyze the polymer's chemical structure. Samples contained 20 mg of dried polymer dissolved in $CDCl_3$. The chemical shifts are given in ppm downfield from tetramethylsilane (TMS), as shown in Figure S1. ^{1}H NMR ($CDCl_3$ with 0.05% v/v TMS, 400 MHz): δ = 7.85 (4Ha, m, J = 9 Hz), 7.24 (4Hb, m, J = 9 Hz), 7.01 (4Hc, m, J = 9 Hz), 6.94 (4Hd, m, J = 9 Hz), 1.69 (6He, s).

In order to determine the molecular weight of the copolymers, size exclusion chromatography (SEC) was performed using a Waters Alliance e2695 HPLC system, with Styragel® HR5 and HR4 7.8×300 mm (THF) columns in series, interfaced to a light scattering detector (miniDAWN TREOS) and an Optilab T-rEX differential refractive index (dRI) detector. The mobile phase was THF Optima (inhibitor-free) at a flow rate of 1.0 mL min^{-1}, and samples were calibrated against Pressure Chemical Company low dispersity polystyrene standards of 30 kDa and 200 kDa using Astra v6.1 software. Then, ~1.0 mg mL^{-1} filtered solutions of polymer in THF were prepared for SEC.

Density functional theory calculations

Density functional theory (DFT) calculations, as implemented in GAMESS[23,24] using the M06-2X functional,[25] a 6-311G**(+) basis set, and DMSO implicit solvent were used to calculate the reaction mechanism of the aryl halide condensation reaction through both second- and third-order mechanisms. Truncated monomers were used to represent the polymer, as shown in Figure 3, with Na^+ rather than K^+ to save computational time. Experimental results validated no change in reaction order was caused by interchanging Na^+ and K^+ (discussed below).

Results and Discussion

In a polycondensation reaction between bifunctional A-A and B-B monomers where the stoichiometric ratio ([BPA]:[DXDPS], r) is 1:1, the Carothers equation predicts an infinite degree of polymerization and molecular weight.[26–28] However, in the present work, high molecular weight was not achieved at a 1:1 stoichiometry. To determine the optimal non-stoichiometric ratio to achieve high molar mass polymers, therefore, we first conducted a series of polycondensations of BPA and DCDPS, as well as BPA and DFDPS at various molar ratios (**Scheme 1**). Initial reactions were performed with DCDPS and BPA and are shown in **Figure 1a**. When DCDPS and BPA reacted at 180 ˚C for 48 h with a stoichiometric ratio of r = BPA:DCDPS = 1, a number-averaged molecular weight (M_n) of 17.3 kDa and molecular weight distribution (Đ) of 1.21 were obtained, which is much lower than the Đ of 2.0 predicted for a polycondensation product at full conversion. Then, a moderate excess of DCDPS was used in new reactions under identical reaction conditions (i.e., solvent/monomer concentration, temperature), and the highest molecular weights were observed at r = 0.94 ~ 0.97. In this case, an excess of DCDPS means that low conversion oligomers have two ArCl end groups. We predict that a fraction of the excess –Cl group is hydrolyzed to a –OH group, which achieves a 1:1 stoichiometry in situ. Thus, an optimum conversion and a high molecular weight are obtained during the reaction. It is worth noting that the DCDPS/BPA polymerization exhibited an optimum Đ of ~1.6 at the offset r = 0.94, which suggests that low molecular weight oligomers are still present. Thus, the reaction could be further improved (e.g., increased time, temperature, concentration, etc.) in order to obtain complete conversion. The same phenomenon, an increased X_n via stoichiometric imbalance, was observed in the polymerization with DFDPS (**Figure 1b**, at 140 ˚C for 4 h), where the highest M_n (33 kDa) and Đ (1.93) were observed at r = 0.94. Thus, an optimal stoichiometric ratio of 1:0.94 DXDPS:BPA was utilized for all subsequent reactions discussed. However, the complete conversion obtained for the DFDPS/BPA reaction prompted a subsequent kinetic study to better understand the polymerization behavior of the two aryl halides.

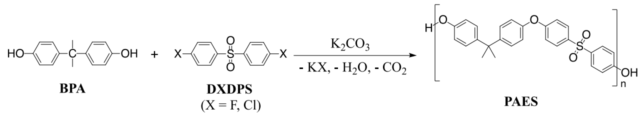

Scheme 1. Typical polycondensation to prepare poly(arylene ether sulfone)s.

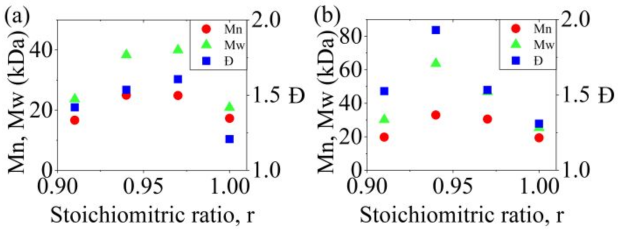

Figure 1. The effect of BPA:DXDPS stoichiometry (r) on the molecular weight and Đ obtained during polycondensation reactions of (a) DCDPS/BPA at 180 ˚C for 48 h and (b) DFDPS/BPA at 140 ˚C for 4 h.

The reaction conversion for the polycondensations utilizing both aryl halides was monitored as a function of time (**Figure 2**). Aliquots were collected from the reactor until the reaction reached completion. Importantly, it took around 4 h for the DFDPS/BPA polycondensation to reach the high conversion plateau, while the DCDPS/BPA reaction took up to 48 h under identical experimental conditions. Next, the conversion data was linearized using integer rate law expressions. The DCDPS/BPA polymerization showed linearity when fit with a second order rate expression, as seen in **Figure 3a**. This corroborates previous literature[17] that describes the mechanism of the condensation polymerization to form PAES via the S_NAr mechanism. In the DFDPS/BPA reaction, the reaction rate constant is significantly higher than that of the DCDPS/BPA reaction under identical experimental conditions due to the relatively higher electronegativity and smaller size of fluorine.[16] Interestingly, the DFDPS/BPA polymerization has a reaction order higher than second order (**Figure 3b**). Specifically, the data are described fairly well with a third-order rate expression, suggesting that the reaction is second order with respect to either DFDPS or BPA. We hypothesize that the relatively higher electronegativity of the fluorine attracts two phenolate salts to make the reaction second order with respect to BPA and first order with respect to DFDPS. This hypothesis was tested using computational and experimental means. As a final note, overall, the third-order rate expression describes the reaction progression well, but deviations were observed at lower reaction times. This phenomenon was further examined and is discussed below.

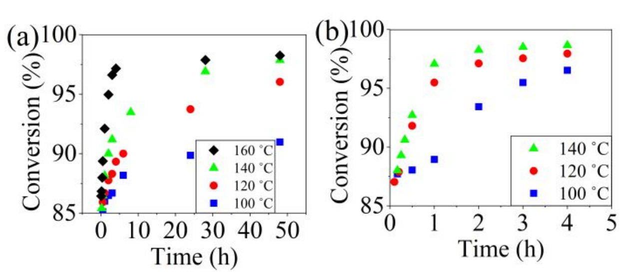

Figure 2. Plots of reaction conversion versus time for the polymerization of: (a) DCDPS and BPA, and (b) DFDPS and BPA at various temperatures with K_2CO_3.

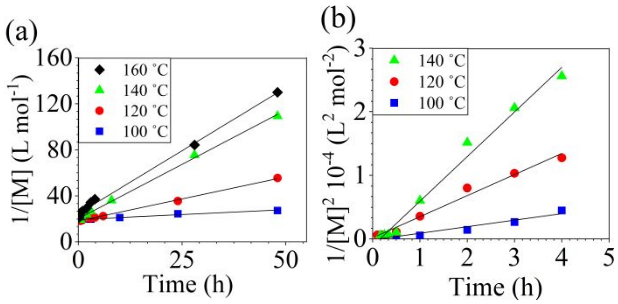

Figure 3. Linearized kinetic plots of: (a) second-order reaction for the DCDPS/BPA polycondensation, and (b) third-order reaction for the DFDPS/BPA polycondensation at various temperatures with K_2CO_3.

Viswanathan and McGrath[29] studied the reaction of DCDPS/BPA in *N*,*N*-dimethylacetamide (DMAc) and toluene (at a 1:1 volumetric ratio) and catalyzed by K_2CO_3. They observed non-linear kinetics when plotting conversion versus the inverse of concentration with an apparent reaction order less than two. They attributed this deviation to the partially heterogeneous nature of the reaction (i.e., the K_2CO_3 is only partially soluble). In the present work, however, DMSO and toluene (at a 4:1 volumetric ratio) was used as the solvent, which improved the solubility of K_2CO_3 and also the overall dielectric constant of the reaction medium, thus a linear second order kinetic plot was observed in the DCDPS/BPA reaction. The DFDPS/BPA reaction, however, displayed a reaction order greater than two. Therefore, the mechanism for the DFDPS/BPA polycondensation is independent of the limited solubility of K_2CO_3 and is different than the classical S_NAr mechanism.

Additionally, polycondensation reactions with sodium carbonate (Na_2CO_3) as the base were also performed for combinations of both DCDPS/BPA and DFDPS/BPA. A steady increase in molecular weight was observed, though at a slower reaction rate, as expected. Two factors that contribute to the slower reaction are the relatively lower solubility of Na_2CO_3 in DMSO and the lower reactivity of the sodium phenolate compared to potassium phenolate. The SEC elution traces and time-dependent plots of conversion are seen in **Figures S5-6**. The conversion data were linearized (**Figure 4**) and a good fit to a second-order rate law for the DCDPS/BPA reaction was observed with Na_2CO_3 whereas the DFDPS/BPA reaction followed a third order rate expression. These observations match the polymerizations performed using K_2CO_3 as a base and eliminate the possibility that the counterion influenced the reaction order.

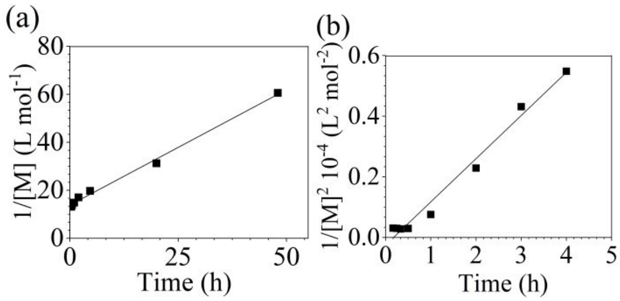

Figure 4. Linearized kinetic plots of: (a) second-order reaction for the polycondensation of DCDPS/BPA with Na_2CO_3 at 160 ˚C, and (b) third-order reaction for the polycondensation of DFDPS/BPA with Na_2CO_3 at 140 ˚C.

To review, the mechanism for the classical S_NAr reaction is shown in **Scheme 2**. Following the formation of the phenolate ion a complex between the cation and the aryl halide forms. The phenolate then attacks the aryl halide to form the Meisenheimer complex, which then goes on to form the arylene ether. However, the observations above suggest a higher order reaction pathway when the aryl halide contains a fluorine. Therefore, a mechanism for the third-order reaction between DFDPS and BPA is proposed in **Scheme 3**. In this reaction pathway, the main difference is the formation of a three-body complex wherein two phenolates are interacting with the ArF. One of the phenolates continues activating the ArF while the other attacks causing the formation of the Meisenheimer complex. Then, aromaticity is reformed as the arylene ether is created. Importantly, though not captured in **Scheme 3**, the potassium ion can exist as either a free ion or as a part of the phenolate complex shown in **Schemes 2** and **3**. For the sake of clarity, the potassium ion, in either form, is referred to as “B” in the subsequent discussions.

To probe the plausibility of this reaction pathway, DFT calculations were used to study the reaction. The kinetic data using potassium and sodium counterions suggested that sodium could be used to save computational time. Thus, the “B” noted above is used to denote a sodium ion in the DFT discussion below. Interestingly, previous computational work[30,31] showed that potassium cresolate formed a two-body complex with an ArF as an intermediate of the nucleophilic substitution reaction. However, the possibility of a three-body complex was not considered or reported. The DFT calculations of the relative formation energies of the intermediate complexes and final products in the DFDPS/BPA and DCDPS/BPA reactions suggest that the formation of a single three-body ArX•••2B complex (-131 kJ/mol) is strongly favorable over forming a two-body ArX•••B complex (-23 kJ/mol, **Figure 5**). The DFT results go on to show that the activation barrier to form the Meisenheimer transition state for the three-body ArCl•••2B reaction is 85 kJ/mol, which is significantly higher than that of the two-body ArCl•••B complex (68.3 kJ/mol). For the ArF monomer, the activation barriers are similar (52 and 59 kJ/mol for the two-body and three-body complexes, respectively). Together, this predicts that the ArCl reaction will proceed through the energetically more favorable two-body path (**Scheme 2**, in agreement with the experimental second-order kinetics) and the ArF reaction will proceed through the three-body pathway (**Scheme 3**). The three-body S_NAr pathway has therefore been termed the cation-activated S_NAr pathway.

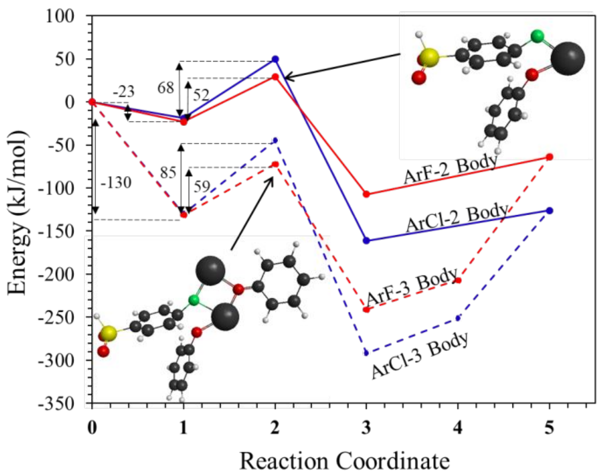

Figure 5. Schematic representation of reaction profiles for ArF (red lines) and ArCl (blue lines) with NaPhO (B) in a two-body complex pathway (solid line) and a three-body complex pathway (dashed line). The reaction coordinates are: 1) complexed reactants, 2) transition state, 3) complexed products, 4) ArX-B complex, 5) fully de-complexed products – Ar-O-Ph and NaX.

The energetics of the complex formation and the reaction calculated using DFT were compared to the experimental data. Performing the polycondensation reactions at varying temperatures enabled the creation of Arrhenius plots for the DFDPS/BPA and DCDPS/BPA reactions (**Figure 6**). The activation energy (E_a) for the DFDPS/BPA reaction was 6.0 kJ/mol lower than the DCDPS/BPA reaction. Also, the pre-exponential factor for the DFDPS/BPA reaction was nearly three orders of magnitude higher than that for the DCDPS/BPA reaction.

Finally, the data revealed that the rate constant was significantly higher for the ArF reaction, as also evidenced by the shorter reaction time need to achieve complete conversion. Together, the DFT calculations, the proposed mechanism (**Scheme 3**), the activation energies, and the pre-exponential factors suggest that the reactions are driven by changes in both enthalpy and entropy. Moreover, the activation energies from the experimental data match in both the order of magnitude and the trend predicted by the DFT calculations. **Table 1** summarizes the relevant kinetic data for the series of polymerizations.

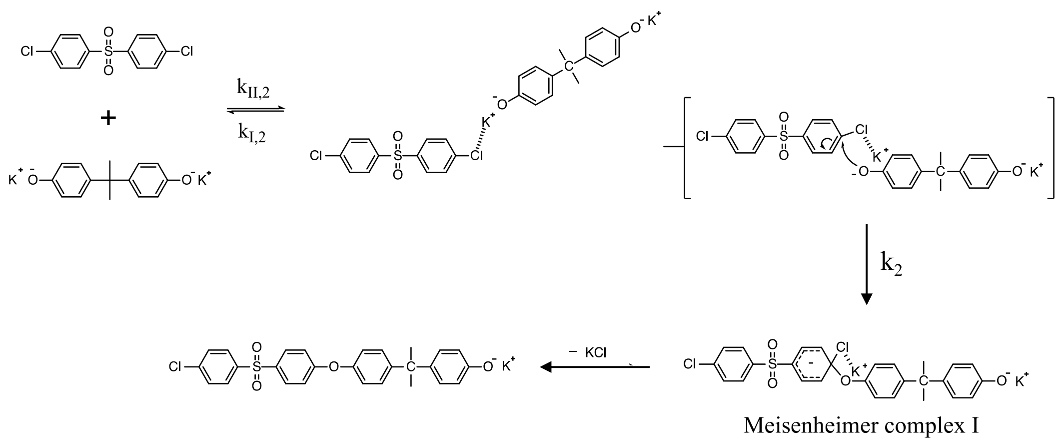

Scheme 2. S_NAr mechanism for the polycondensation ArCl and K^+PhO^- to form PAES.

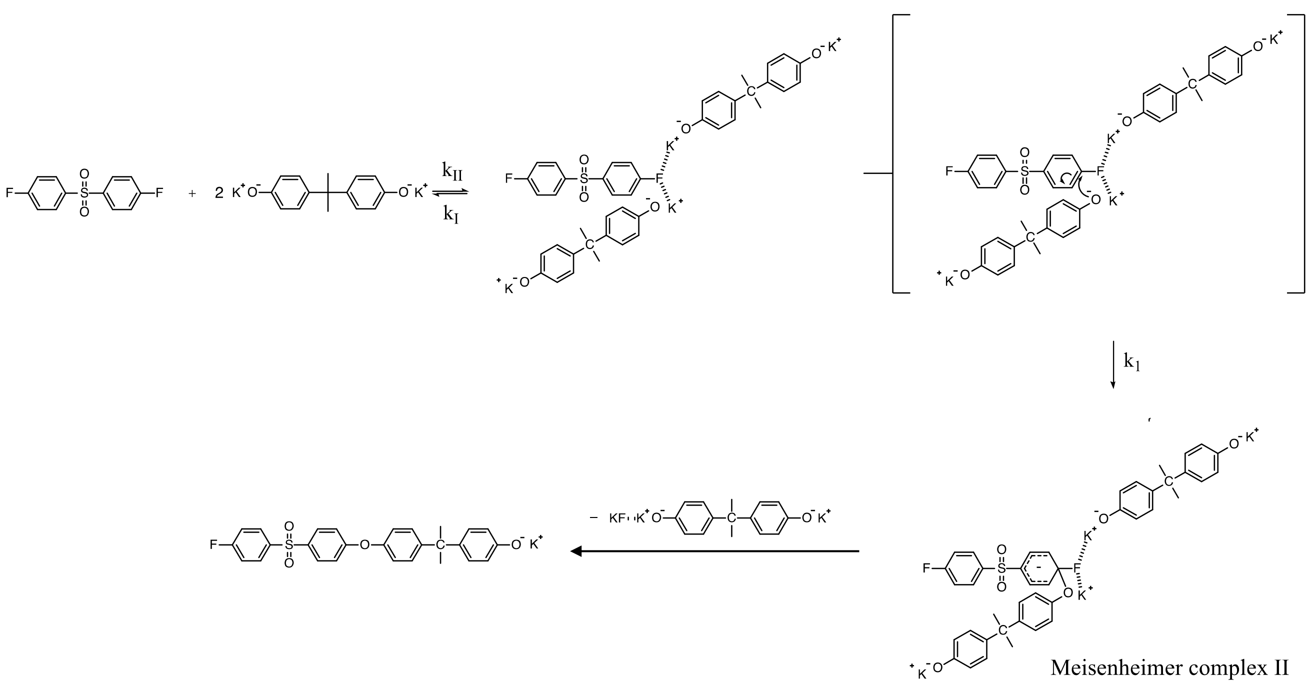

Scheme 3. Potassium-activated S_NAr mechanism for the polycondensation ArF and K^+PhO^- to form PAES.

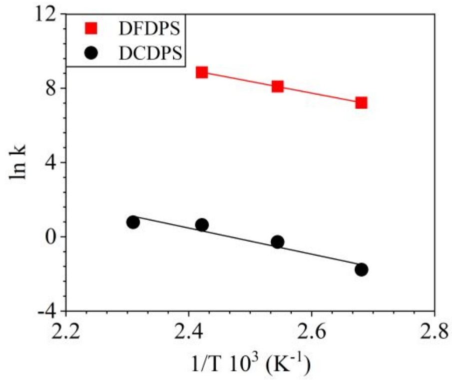

Figure 6. Arrhenius plots for the rate constants of polycondensation reactions of DFDPS/BPA (red square) and DCDPS/BPA (black circle) with K_2CO_3 as the base.

Table 1. Kinetic data for the polycondensation of DFDPS/BPA and DCDPS/BPA with K_2CO_3.

Monomers	Temperature (˚C)	Reaction time (h)	Conversion (%)	k		ln A	E_a (kJ mol^{-1})	*$E_{a,\ DFT}$ (kJ mol^{-1})
DFDPS + BPA	140	4	98.7	7023	L^2 mol $^{-2}$ h^{-1}	24	52	59
	120		97.9	3289				
	100		96.5	1366				
DCDPS + BPA	160	48	98.2	2.2	L mol^{-1} h^{-1}	17	58	69
	140		97.9	1.9				
	120		96.0	0.8				
	100		93.2	0.2				

*: Activation energy obtained through DFT calculation.

The following discussion details an in-depth analysis of the reaction kinetics for the DFDPS/BPA and DCDPS/BPA polymerizations. The energetic analyses from DFT and experimental data indicate that the ArF/BPA reaction proceeds via the formation of a three-body complex (ArF•••2B), which is in equilibrium with ArF and two Bs (at least one of the two Bs is a K^+PhO^-). Whereas, the ArCl/BPA reaction proceeds through a two-body complex (ArCl•••B) via the classical S_NAr mechanism. The equilibrium constants, $K_{a,1}$ and $K_{a,2}$, for the formation of a three-body complex and two-body complex are expressed in Eqs. 1 and 2, respectively:

$$K_{a,1} = \frac{k_{I,1}[ArF \cdots 2B]}{k_{II,1}[ArF][B]^2} \quad (1)$$

$$K_{a,2} = \frac{k_{I,2}[ArCl \cdots B]}{k_{II,2}[ArCl][B]} \quad (2)$$

where $k_{I,1}$ and $k_{I,2}$ are the reverse rate constants and $k_{II,1}$ and $k_{II,2}$ are the forward rate constants in the potassium activation step to form either ArF•••2B (1) or ArCl•••B (2). The concentration of the complex is thus a function of the concentrations of ArX and B. The reaction rate, r, is then directly proportional to the concentrations of the activated complex:

$$r = -\frac{d[M]}{dt} = k_1[ArF \cdots 2B] \quad (3)$$

$$r = -\frac{d[M]}{dt} = k_2[ArCl \cdots B] \quad (4)$$

where k_1 and k_2 are the rate constants, with units of h^{-1}, of the rate limiting step (formation of the Meisenheimer complex) in the DCDPS/BPA reaction (**Scheme 2**) and DFDPS/BPA reaction (**Scheme 3**), respectively.

Combining Eq. 1 and Eq. 3 yields:

$$r = -\frac{d[M]}{dt} = k_1 K_{a,1} \frac{k_{II,1}}{k_{I,1}} [ArF][B]^2 \quad (5)$$

Similarly, combining Eq. 2 and Eq. 4 yields:

$$r = -\frac{d[M]}{dt} = k_1 K_{a,2} \frac{k_{II,2}}{k_{I,2}} [ArCl][B] \quad (6)$$

It is important to note a deviation from the third-order rate law fit was observed in the DFDPS/BPA polymerization at conversions < 90%. However, the DCDPS/BPA polymerization fits the second-order rate law over the whole course of the reaction (Figure 7a). Since the reaction proceeds exponentially with time, this the low-conversion region of DFDPS/BPA polymerization is captured by a relatively small period of time (Figure 7b). According to Flory,[32] the failure to fit the data over the low-conversion region is attributed to the large decrease in the polarity of the reaction medium as the phenolate groups are replaced by the arylene ether groups and the simultaneous removal of water at the initial stage of the reaction. The decrease in polarity alone can induce a change in the order of reaction, which is corroborated by the experimental data shown in **Figure 3b**.

Specifically, the reaction order changes from 2.5 in the low conversion region (**Figure 7b**) to a reaction order of three in the high conversion region, which corresponds to a change in the composition of the three-body complex from $[K^+][K^+PhO^-][ArF]$ in the high polarity medium to $[K^+PhO^-][K^+PhO^-][ArF]$ in the relatively lower polarity medium. This suggests that the free potassium cation is a more effective activator than the paired K^+PhO^- salt in the high polarity, low conversion region, where the concentration of free potassium cation ($[K^+]$) is also relatively high. $[K^+]$ is given by:

$$[K^+] = (K_{k^+PhO^-}[K^+PhO^-])^{1/2} \quad (7)$$

where K_{K+PhO-} is the ionization constant for K^+PhO^-. Combining Eq. 5 and Eq. 7, the reaction rate of the DFDPS/BPA polymerization at low conversion follows an overall 2.5-order rate law, given by:

$$r = -\frac{d[M]}{dt} = k_1 K_{a,1} \frac{k_{II,1}}{k_{I,1}} (K_{K^+PhO^-})^{\frac{1}{2}} [ArF][K^+PhO^-]^{3/2} \ (8)$$

while at higher conversions, in the relatively lower polar reaction medium, the reaction rate of the DFDPS/BPA reaction follows the third-order rate law expressed as:

$$r = -\frac{d[M]}{dt} = k_1 K_{a,1} \frac{k_{II,1}}{k_{I,1}} [ArF][K^+PhO^-]^2 \quad (9)$$

That this phenomenon was only observed for the DFDPS/BPA polymerization, and not the DCDPS/BPA polymerization, provides further evidence for K•••F or Na•••F interaction as well as the reaction mechanism proposed in Scheme 3.

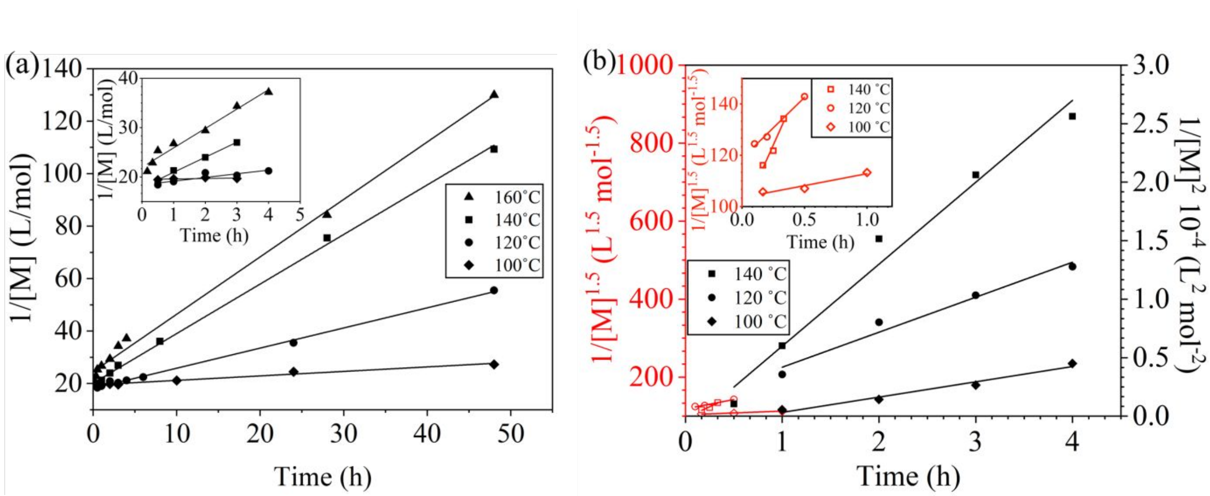

Figure 7. Linearized kinetic plot of (a) the DCDPS/BPA reaction and (b) the DFDPS/BPA reaction at conversions < 90% (hollow red markers) fit to a 2.5-order rate expression (red line), and at conversions > 90% (solid black markers) fit to a third-order rate expression (black line) at various temperatures with potassium carbonate as the base.

The aryl fluoride-potassium interaction was further investigated using NMR spectroscopy. Specifically, K^+PhO^- was prepared and mixed with DFDPS at varying molar ratios under anhydrous conditions, and the chemical shifts of the ^{19}F resonances were observed. The ArF strongly interacted with the potassium ion(s), as seen in **Figure 8**. The ^{19}F NMR spectra revealed that the chemical shift of fluorine increased monotonically as the DFDPS/K^+PhO^- ratio increased. This trend is further supportive that the rate expression is second order with respect to B since the trend continues linearly at stoichiometric ratios less than one. Changes in the chemical shift are the result of a combination of the effects from electron density changes (i.e., diamagnetic) and overlap/interactions between molecular orbitals (i.e., paramagnetic) effects.[33] If the diamagnetic contributions only were analyzed, the increase in chemical shift would suggest a reduction in electron density at the ArF, which is counterintuitive and dissimilar to the proposed cation-activated S_NAr reaction mechanism. Therefore, DFT calculations were utilized again to predict the changes in the charge state of the ArF upon complexation with the Na^+PhO^- (**Table S1**). Note again that the counterion (Na^+ versus K^+) will not affect the phenomenon observed, simply the magnitude of the effect. The negative charge of the fluorine is calculated to increase slightly (0.02 electron) upon the introduction of Na^+PhO^- at ratios of 1:1 and 1:2, based on Bader charge analysis.[34] Although the amount gained is small, we note that the subtlety of electron density change is mirrored in the NMR which also shows only a slight shifts. For the sake of clarity, it is important to note that Bader charge does not necessarily correlate directly with formal charge, as electron sharing is explicitly included; however, it does show that additional electron density localizes on the fluorine of the ArF as each Na^+ complexes with the DFDPS molecule. This additional electron localization on the fluorine of the ArF is consistent with the relative electronegativity of the F and Na as well as the additional charge attraction from the Na^+ it would experience during the formation of the three-body complex in the cation-activated S_NAr reaction. The results of this calculation are consistent with intuition. Thus, the ^{19}F NMR spectroscopy and DFT calculations suggest that a significant paramagnetic effect occurs in the DFDPS/K^+PhO^- complex, which will be the subject of future investigations. In summary, the ^{19}F NMR results (**Figure 8**) and the DFT calculations of electron density distribution confirm the presence of the ArF•••K^+ interaction as well as provide strong support for the cation-activated S_NAr mechanism.

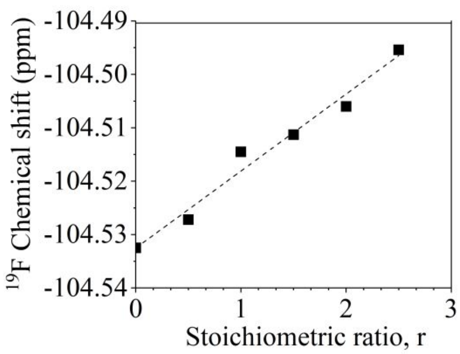

Figure 8. Chemical shifts of the ^{19}F nuclear magnetic resonance upon ArF interactions with K^+PhO^- at various stoichiometric ratios (r, K^+PhO^-:ArF).

Collectively, this finding, that the mechanism of the S_NAr reaction is dependent on the composition of the aryl halide is quite compelling. First, the findings are relevant to commercially relevant PAESs despite the recent move away from BPA-based macromolecules due to concerns over mutagenicity, endocrine disruption, and environmental accumulation; this sustained relevance is due to the effect of the aryl halide on the reaction pathway, not the bisphenol monomer. Moreover, we anticipate that this work could create interest and future endeavors in designing reaction catalysts and optimizing reaction conditions for S_NAr reactions. The polymerization of PAES requires deprotonation of the phenol to produce a good nucleophile, which makes the use of carbonate salts fairly practical. Similarly, the desire to produce polymers of high molecular weight necessitate 1:1 stoichiometries (in situ). However, the opportunity to optimize analogous S_NAr reactions using the outcomes of this work is possible. For example, other potassium salts, such as KPF_6 and $K(CF_3SO_2)N$, are highly soluble in various organic solvents but are only weakly ion paired compared to K_2CO_3. Thus, the ion pairing in the salt and the improved solubility could be used to tune or optimize the reaction rate and improve reaction kinetics in organic solvents like DMSO. We note above that the reaction polarity affects the form of the salt and the reaction order; therefore, ion pairing strength can be used as a functional handle to tune the reaction kinetics.

Conclusions

In conclusion, we report the kinetics and mechanisms of S_NAr of a classic polymer system: PAES prepared using DFDPS and DCDPS with BPA. As expected, the ArCl monomer follows a second-order rate law; however, the S_NAr of ArF follows a third-order rate law. The C-F bond is activated by free alkali cations or alkali-phenolates within energetically favorable three-body [ArF•••2B] complexes, producing a third-order rate law and alternate cation-activated S_NAr mechanism. The C-Cl bond is activated by an alkali-phenolate that favors a two-body [ArCl•••B] complex, producing a second-order rate law following the classical S_NAr mechanism. This conclusion is supported by experimental observation and computational calculation for both potassium-activated reactions and sodium-activated reactions. Our results provide additional understanding of polycondensation mechanisms for aryl halide monomers as well as support the importance of C-X interactions with dissociated alkali ions and alkali-containing charge complexes. Further exploration of the polycondensation medium effects on the overall reaction behavior as well as the applications of this discovery to the synthesis of other arylene ethers is under investigation.

Electronic Supplementary Information. Information in the electronic supplementary information includes: details regarding characterization tools and procedures, ^{1}H NMR spectra, size exclusion chromatography traces, off-set stoichiometry study, DFT calculation protocols, and kinetic data for polycondensation reactions in the presence of sodium carbonate.

Conflicts of Interest

The authors declare no competing financial interest.

Acknowledgements

The authors acknowledge Prof. Jeffery L. Yarger, Dr. Brian R. Cherry, and Dr. Stephen K. Davidowski at ASU for helpful discussions. This work was financially supported by NSF CBET 1836719, NASA ECF (80NSSC18K1508), and ARPA-E (DE- AR0001103). This work used the Extreme Science and Engineering Discovery Environment (XSEDE) through allocation ECD190001.

Notes

*Corresponding Author: E-mail address: mdgreen8@asu.edu (M.D. Green)

References

(1) Kricheldorf, H. R. What Does Polycondensation Mean? In *Macromolecular Symposia*; 2003; Vol. 199, pp 1–13. https://doi.org/10.1002/masy.200350901.

(2) Noshay, A.; Robeson, L. M. Sulfonated Polysulfone. *J. Appl. Polym. Sci.* **1976**, *20* (7), 1885–1903. https://doi.org/10.1002/app.1976.070200717.

(3) Zhao, C.; Xue, J.; Ran, F.; Sun, S. Modification of Polyethersulfone Membranes - A Review of Methods. *Prog. Mater. Sci.* **2013**, *58* (1), 76–150. https://doi.org/10.1016/j.pmatsci.2012.07.002.

(4) Kricheldorf, H. R.; Vakhtangishvili, L.; Fritsch, D. Synthesis and Functionalization of Poly(Ether Sulfone)s Based on 1,1,1-Tris(4-Hydroxyphenyl)Ethane. *J. Polym. Sci. Part A Polym. Chem.* **2002**, *40* (17), 2967–2978. https://doi.org/10.1002/pola.10372.

(5) Ren, J.; O'Grady, B.; deJesus, G.; McCutcheon, J. R. Sulfonated Polysulfone Supported High Performance Thin Film Composite Membranes for Forward Osmosis. *Polym. (United Kingdom)* **2016**, *103*, 486–497. https://doi.org/10.1016/j.polymer.2016.02.058.

(6) Wang, F.; Glass, T.; Li, X.; Hickner, M.; Kim, Y. S.; McGrath, J. Synthesis and Characterization of Controlled Molecular Weight Poly(Arylene Ether Sulfone) Copolymers Bearing Sulfonate Groups by Endgroup Analysis. In *American Chemical Society, Polymer Preprints, Division of Polymer Chemistry*; 2002; Vol. 43, pp 492–493.

(7) Harrison, W. L.; O'Connor, K.; Arnett, N.; McGrath, J. E. Homogeneous Synthesis and Characterization of Sulfonated Poly(Arylene Ether Sulfone)s via Chlorosulfonic Acid. In *American Chemical Society, Polymer Preprints, Division of Polymer Chemistry*; 2002; Vol. 43, p 1159.

(8) Johnson, B. C.; Yilgör, İ.; Tran, C.; Iqbal, M.; Wightman, J. P.; Lloyd, D. R.; McGrath, J. E. Synthesis and Characterization of Sulfonated Poly(Acrylene Ether Sulfones). *J. Polym. Sci. Polym. Chem. Ed.* **1984**, *22* (3), 721–737. https://doi.org/10.1002/pol.1984.170220320.

(9) Robeson, L. M.; Farnham, A. G.; McGrath, J. E. Synthesis and Dynamic Mechanical Characteristics of Poly(Aryl Ethers). *Appl. Polym. Symp.* **1975**, *26* (polym. polycondensat), 375–385.

(10) Dennis, J. M.; Fahs, G. B.; Moore, R. B.; Turner, S. R.; Long, T. E. Synthesis and Characterization of Polysulfone-Containing Poly(Butylene Terephthalate) Segmented Block Copolymers. *Macromolecules* **2014**, *47* (23), 8171–8177. https://doi.org/10.1021/ma501903h.

(11) Duncan, A. J.; Layman, J. M.; Cashion, M. P.; Leo, D. J.; Long, T. E. Oligomeric A2+ B3synthesis of Highly Branched Polysulfone Ionomers: Novel Candidates for Ionic Polymer Transducers. *Polym. Int.* **2010**, *59* (1), 25–35. https://doi.org/10.1002/pi.2684.

(12) Suga, T.; Wi, S.; Long, T. E. Synthesis of Diazocine-Containing Poly(Arylene Ether Sulfone)s for Tailored Mechanical and Electrochemical Performance. *Macromolecules* **2009**, *42* (5), 1526–1532. https://doi.org/10.1021/ma802249a.

(13) Kricheldorf, H. R.; Böhme, S.; Schwarz, G.; Krüger, R. P.; Schulz, G. Macrocycles. 18. The Role of Cyclization in Syntheses of Poly(Ether-Sulfone)S. *Macromolecules* **2001**, *34* (26), 8886–8893. https://doi.org/10.1021/ma010218l.

(14) Sahre, K.; Hoffmann, T.; Pospiech, D.; Eichhorn, K. J.; Fischer, D.; Voit, B. Monitoring of the Polycondensation Reaction of Bisphenol A and 4,4′-Dichlorodiphenylsulfone towards Polysulfone (PSU) by Real-Time ATR-FTIR Spectroscopy. *Eur. Polym. J.* **2006**, *42* (10), 2292–2301. https://doi.org/10.1016/j.eurpolymj.2006.05.025.

(15) Jennings, B. E.; Jones, M. E. B.; Rose, J. B. Synthesis of Poly(Arylene Sulfones) and Poly(Arylene Ketones) by Reactions Involving Substitution at Aromatic Nuclei. *J. Polym. Sci. Polym. Symp.* **1967**, *16*

(Pt. 2), 715–724. https://doi.org/10.1002/polc.5070160212.

(16) Bunnett, J. F. Aromatic Substitution by the SRN1 Mechanism. *Acc. Chem. Res.* **1978**, *11* (11), 413–420. https://doi.org/10.1021/ar50131a003.

(17) Bunnett, J. F.; Zahler, R. E. Aromatic Nucleophilic Substitution Reactions. *Chem. Rev.* **1951**, *49* (2), 273–412. https://doi.org/10.1021/cr60153a002.

(18) Ganguly, S.; Gibson, H. W. Synthesis of a Novel Macrocyclic Arylene Ether Sulfone. *Macromolecules* **1993**, *26* (10), 2408–2412. https://doi.org/10.1021/ma00062a003.

(19) Ross, S. D. Nucleophilic Aromatic Substitution Reactions. In *Progress in Physical Organic Chemistry*; 2007; Vol. 1, pp 31–74. https://doi.org/10.1002/9780470171806.ch2.

(20) Ross, S. D. Catalysis of Intermediate Formation in Nucleophilic Aromatic Substitution. *Tetrahedron* **1969**, *25* (18), 4427–4436. https://doi.org/10.1016/S0040-4020(01)82984-7.

(21) Ross, S. D.; Finkelstein, M.; Petersen, R. C. Nucleophilic Displacement Reactions in Aromatic Systems. V. The Mechanism of the Reaction of 2,4-Dinitrochlorobenzene with Primary Amines in Chloroform. *J. Am. Chem. Soc.* **1959**, *81* (20), 5336–5342. https://doi.org/10.1021/ja01529a024.

(22) Jones, G. O.; Al Somaa, A.; O'Brien, J. M.; Albishi, H.; Al-Megren, H. A.; Alabdulrahman, A. M.; Alsewailem, F. D.; Hedrick, J. L.; Rice, J. E.; Horn, H. W. Computational Investigations on Base-Catalyzed Diaryl Ether Formation. *J. Org. Chem.* **2013**. https://doi.org/10.1021/jo400550c.

(23) Gordon, M. S.; Schmidt, M. W. Chapter 41 - Advances in Electronic Structure Theory: GAMESS a Decade Later; Dykstra, C. E., Frenking, G., Kim, K. S., Scuseria, G. E. B. T.-T. and A. of C. C., Eds.; Elsevier: Amsterdam, 2005; pp 1167–1189. https://doi.org/https://doi.org/10.1016/B978-044451719-7/50084-6.

(24) Schmidt, M. W.; Baldridge, K. K.; Boatz, J. A.; Elbert, S. T.; Gordon, M. S.; Jensen, J. H.; Koseki, S.; Matsunaga, N.; Nguyen, K. A.; Su, S.; Windus, T. L.; Dupuis, M.; Montgomery Jr, J. A.; Schmidt, M. W.; Baldridge, K. K.; Boatz, J. A.; Elbert, S. T.; Gordon, M. S.; Jensen, J. H.; Koseki, S.; Matsunaga, N.; Nguyen, K. A.; Su, S.; Windus, T. L.; Dupuis, M.; Montgomery, J. A. General Atomic and Molecular Electronic Structure System. *J. Comput. Chem.* **1993**, *14* (11), 1347–1363. https://doi.org/10.1002/jcc.540141112.

(25) Truhlar, D. G. The M06 Suite of Density Functionals for Main Group Thermochemistry, Thermochemical Kinetics, Noncovalent Interactions, Excited States, and Transition Elements: Two New Functionals and Systematic Testing of Four M06-Class Functionals and 12 Other Function. *Theoretical chemistry accounts.* Berlin 2008, pp 215–241.

(26) Severnyi, V. V.; Minsker, Y. I.; Ovechkina, N. A. Processes Occurring in Organosilicon Compositions Undergoing Vulcanization by Atmospheric Moisture. *Polym. Sci. U.S.S.R.* **1977**, *19* (1), 42–49. https://doi.org/10.1016/0032-3950(77)90146-0.

(27) Nomura, N.; Tsurugi, K.; RajanBabu, T. V.; Kondo, T. Homogeneous Two-Component Polycondensation without Strict Stoichiometric Balance via the Tsuji-Trost Reaction: Remote Control of Two Reaction Sites by Catalysis. *J. Am. Chem. Soc.* **2004**, *126* (17), 5354–5355. https://doi.org/10.1021/ja0492743.

(28) Dove, A. P.; Meier, M. A. R. Step-Growth Polymerization in the 21st Century. *Macromolecular Chemistry and Physics*. 2014, pp 2135–2137. https://doi.org/10.1002/macp.201400512.

(29) Viswanathan, R.; Johnson, B. C.; McGrath, J. E. Synthesis, Kinetic Observations and Characteristics of Polyarylene Ether Sulphones Prepared via a Potassium Carbonate DMAC Process. *Polymer (Guildf).* **1984**. https://doi.org/10.1016/0032-3861(84)90258-1.

(30) Plenio, H. The Coordination Chemistry of the CF Unit in Fluorocarbons. *Chem. Rev.* **1997**, *97* (8), 3363–3384. https://doi.org/10.1021/cr970465g.

(31) Costello, C. A.; McCarthy, T. J. Surface-Selective Introduction of Specific Functionalities onto Poly (Tetrafluoroethylene. *Macromolecules* **1987**, *20* (11), 2819–2828. https://doi.org/10.1021/ma00177a030.

(32) Odian, G. *Principles of Polymerization, 4th Edition*; 2004. https://doi.org/10.1016/B978-1-85617-803-7.50022-5.

(33) Dahanayake, J. N.; Kasireddy, C.; Karnes, J. P.; Verma, R.; Steinert, R. M.; Hildebrandt, D.; Hull, O. A.; Ellis, J. M.; Mitchell-Koch, K. R. Progress in Our Understanding of 19F Chemical Shifts. In *Annual Reports on NMR Spectroscopy*; 2018. https://doi.org/10.1016/bs.arnmr.2017.08.002.

(34) Henkelman, G.; Arnaldsson, A.; Jónsson, H. A Fast and Robust Algorithm for Bader Decomposition of Charge Density. *Comput. Mater. Sci.* **2006**, *36* (3), 354–360.

Table of Contents Entry:

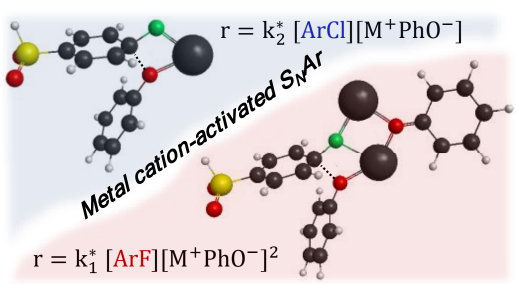

Computational and experimental verification of a second-order rate expression for polysulfones synthesized using diphenyldichloro sulfone versus a third-order rate expression for polysulfones synthesized using diphenyldifluoro sulfone.

Electronic Supplementary Information

Kinetics and mechanisms of polycondensation reactions between aryl halides and bisphenol A

Yi Yang, Christopher L. Muhich, Matthew D. Green*

Department of Chemical Engineering,
School for Engineering of Matter, Transport and Energy,
Arizona State University, Tempe, AZ 85287, USA
***Email: mdgreen8@asu.edu (M.D. Green)**

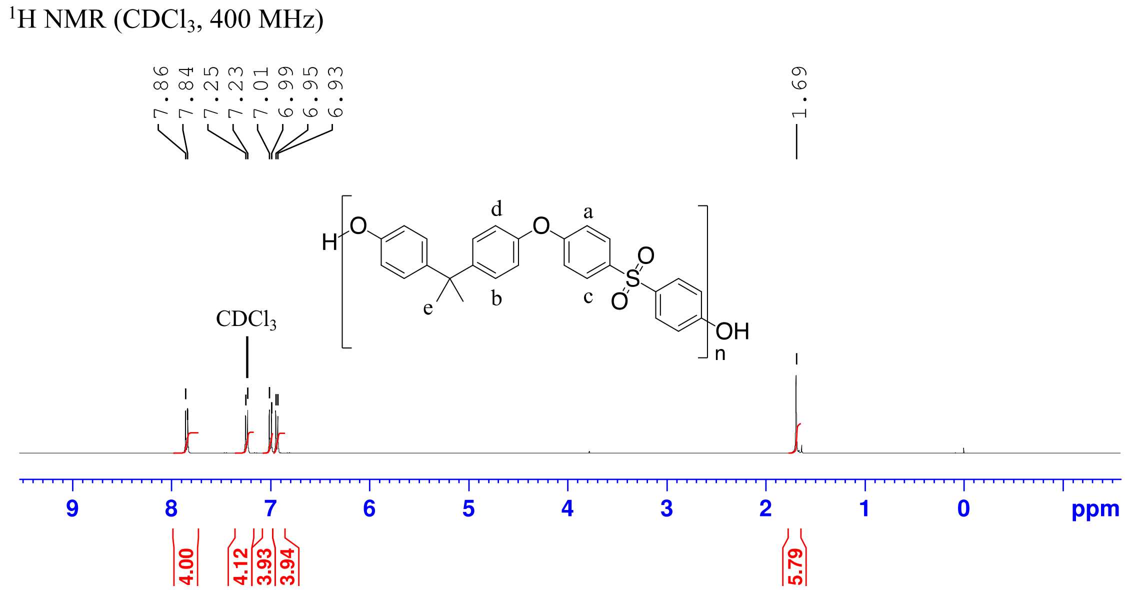

Figure S1. ^{1}H-NMR spectra (CDCl$_3$, 400 MHz) of a representative poly(arylene ether sulfone).

The following details the technique used to determine the kinetics (reaction conversion vs. reaction time) as well as the actual monomer concentrations. An example from the DFDPS/BPA reaction at 140 ˚C is provided. Aliquots were taken at 10 min, 15 min, 20 min, 30 min, 60 min, 120 min, 180 min, and 240 min from the beginning of the reaction, respectively. The number average molecular weight of the product from each aliquot was measured by SEC. The degree of polymerization was calculated from Mn by $X_n=M_n/M_0$, where M_0 is the molecular weight of the repeat unit of polysulfone as 442 g/mol. Then the conversion, p, was calculated as $p = 1-1/X_n$, when the stoichiometric ratio was assumed to be 1 after the hydrolysis side-reaction was compensated by the initial access amount of halide monomers. In terms of monomer concentration, the initial monomer concentration was set as 9.47 mmol/30.5 mL of solvents; the amount of monomer when each aliquot was taken for SEC was calculated as n[M] = 9.47 * (1-p), and the total volume of the solvent at the moment V was taken as the difference between the initial volume of the solvents (V_0 = 30.5 ml) and the distilled solvents/water mixtures collected in the trap (V_d), as well as the amount of the aliquot taken each time (V_a), that is, $V = V_0 - V_d - V_a$; thus, the concentration of the monomer over the course of the reaction was calculated as [M] = n[M]/V from the values given above.

All relevant SEC traces for DFDPS polymerizations are shown in Figure S2, for DCDPS polymerizations are shown in Figure S3.

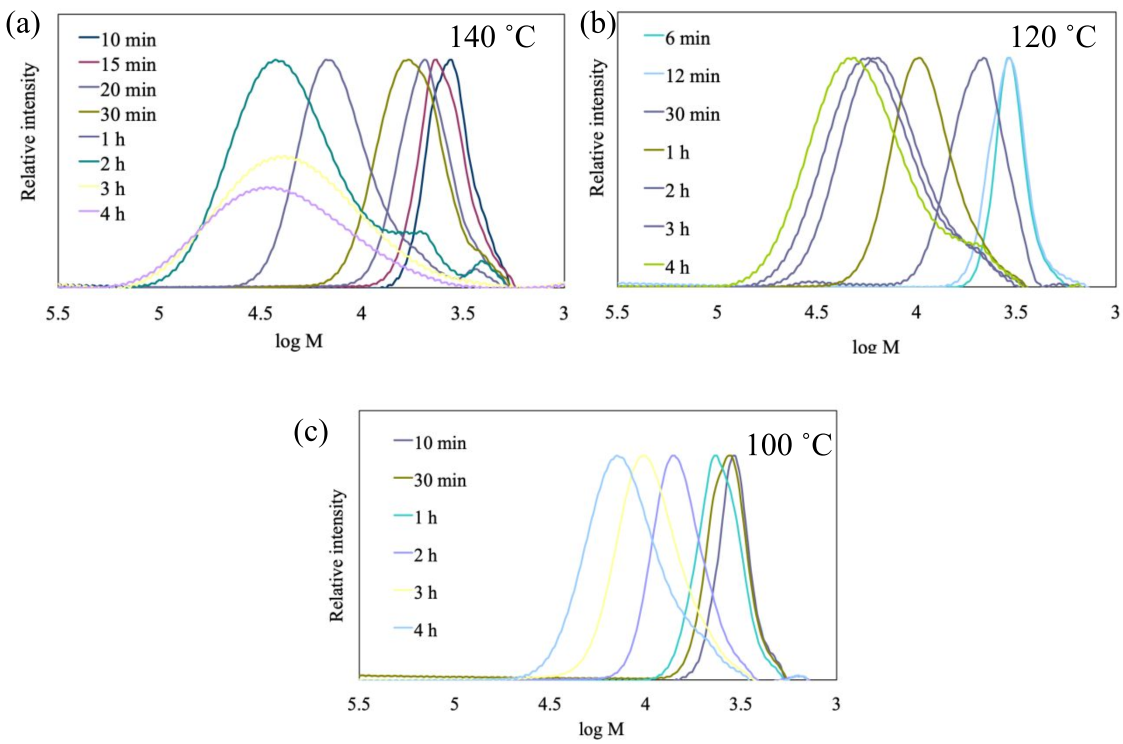

Figure S2. Size exclusion chromatography traces of poly(arylene ether sulfone)s from DFDPS/BPA polycondensation reactions with potassium carbonate performed at (a) 140 ˚C, (b) 120 ˚C, and (c) 100 ˚C as a function of time.

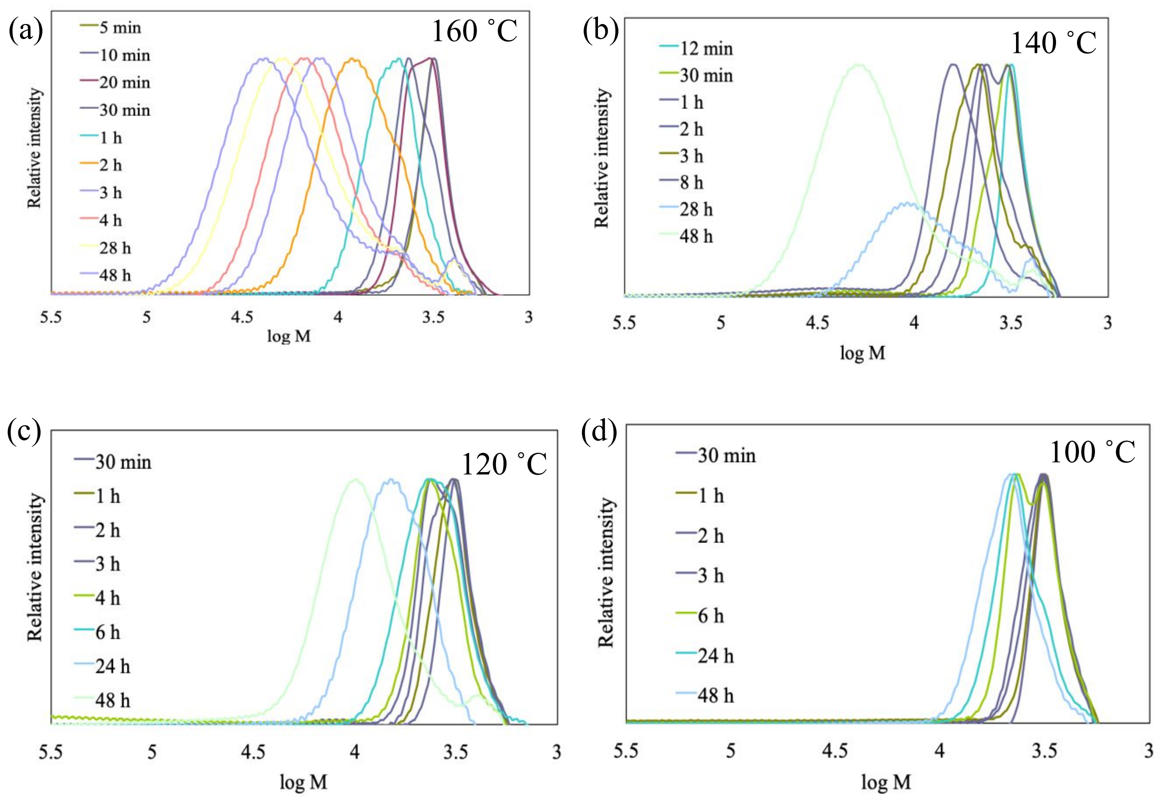

Figure S3. Size exclusion chromatography traces of poly(arylene ether sulfone)s from the DCDPS/BPA polycondensation reactions with potassium carbonate performed at (a) 160 ˚C, (b) 140 ˚C, (c) 120 ˚C, and (d) 100 ˚C as a function of time.

The evolution of Mn versus conversion for the DCDPS/BPA and DFDPS/BPA reactions are shown in Figure S4. These plots follow the classic plots predicted for step-growth polymerizations, wherein high conversion is needed to obtain a high molecular weight polymer.

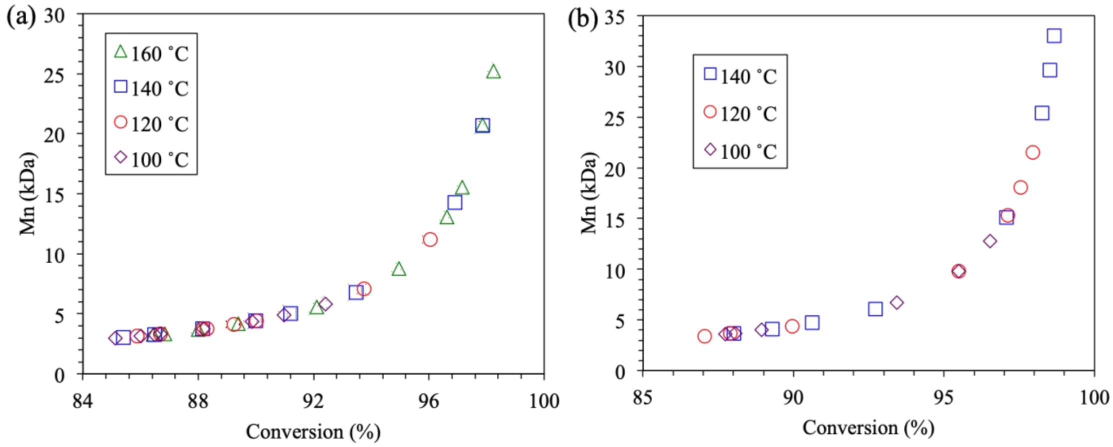

Figure S4. Number-averaged molecular weight (M_n) vs. reaction conversion for the polycondensation of: (a) DCDPS/BPA, and (b) DFDPS/BPA at various temperatures with K_2CO_3. Both plots for the DCDPS/BPA and DFDPS/BPA reactions showed typical step-growth polymerization behavior.

Polycondensation reactions with sodium carbonate as the base were performed for both DCDPS/BPA and DFDPS/BPA (Figure S5-6). The reaction rate of the polymerization with sodium carbonate is relatively lower than reactions that used potassium carbonate under identical experimental conditions. Importantly, the DFDPS/BPA reaction followed the same 2.5-order rate expression at lower conversions and a third-order rate expression at higher conversion. Similarly, a good fit to a second-order rate law for the DCDPS/BPA reaction was observed with sodium carbonate. Thus, it is confirmed that the change of the alkali metal in the base, in this case, is still compatible with the proposed mechanisms.

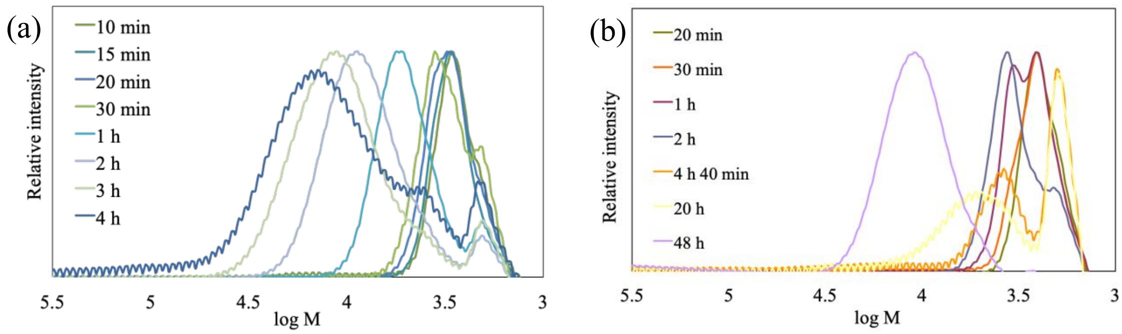

Figure S5. Size exclusion chromatography traces of poly(arylene ether sulfone)s from (a) the DFDPS/BPA polycondensation with sodium carbonate as a function of time at 140 ˚C, and (b) the DCDPS/BPA polycondensation with sodium carbonate as a function of time at 160 ˚C.

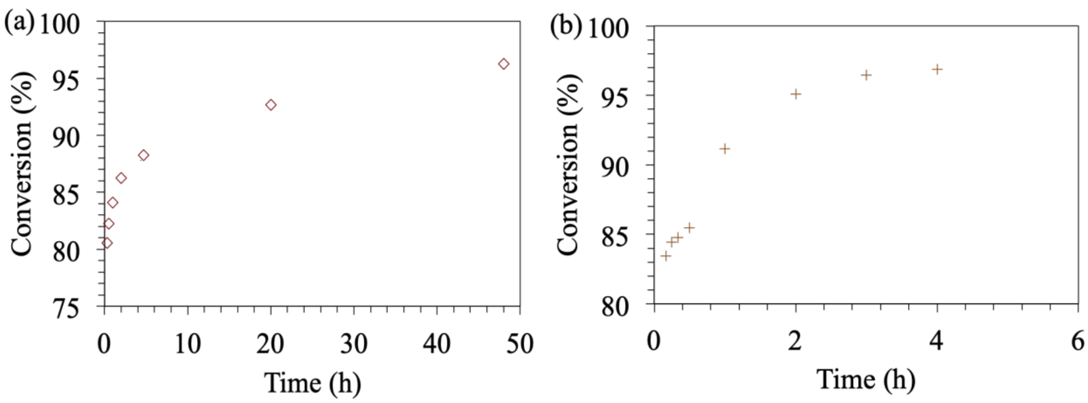

Figure S6. Conversion vs. reaction time plots for the polycondensation of: (a) DCDPS/BPA with sodium carbonate as the base at 160 ˚C, and (b) DFDPS/BPA with sodium carbonate as the base at 140 ˚C.

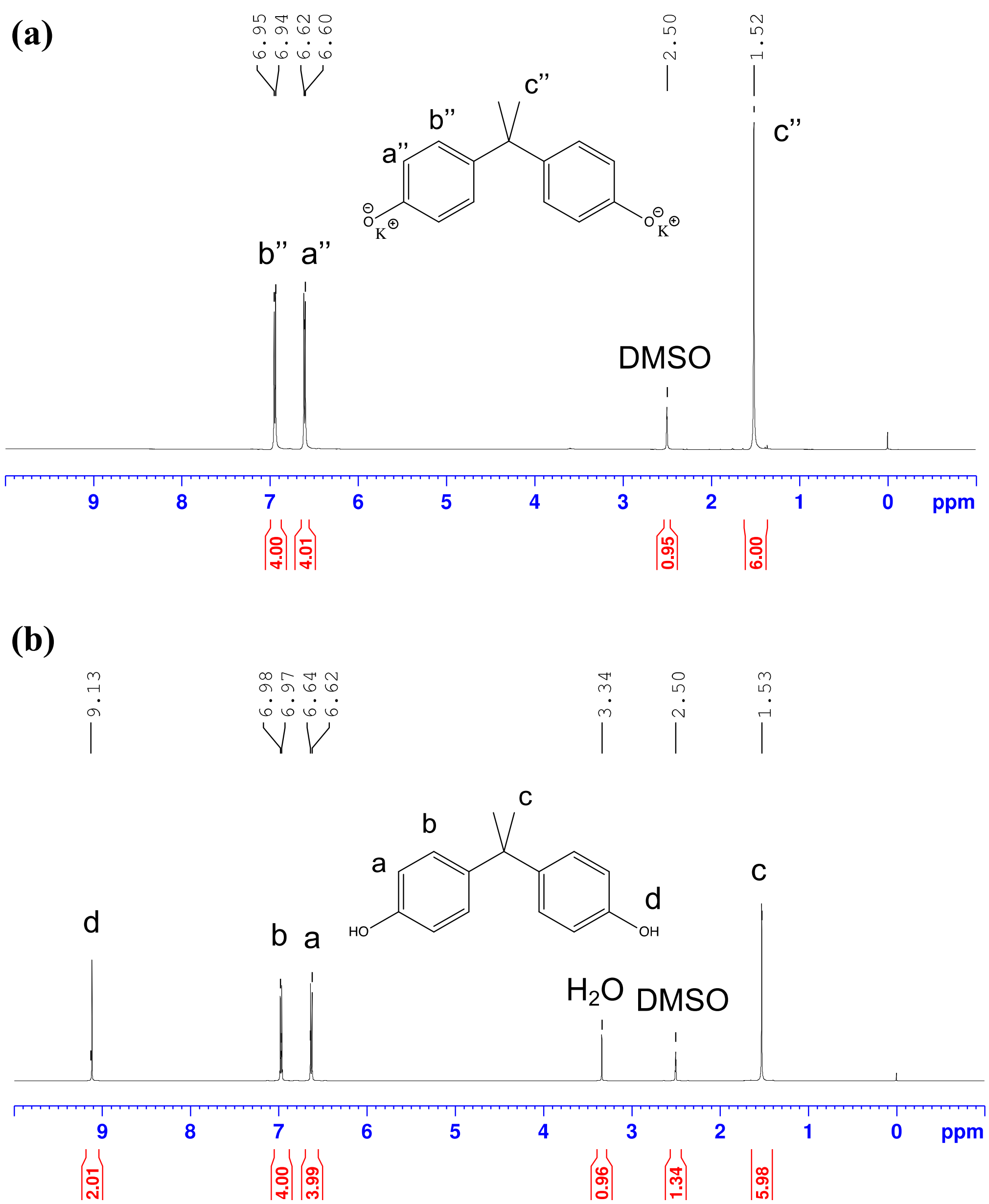

Figure S7. ^{1}H-NMR spectra (DMSO-d_6, 400 MHz) of (a) potassium phenolate and (b) bisphenol A.

In order to experimentally verify the interaction between the aryl fluoride and the potassium ion(s) from species B, potassium phenolate salt was first synthesized. To examine the synthesized potassium phenolate precursor's chemical structure in ^{1}H NMR spectroscopy, deuterated dimethyl sulfoxide (DMSO-d_6) was used as the solvent for both the synthesized K^+PhO^- and bisphenol A. Samples contained 20 mg of dried monomer/precursor dissolved in DMSO-d_6. The chemical shifts are given in ppm downfield from tetramethylsilane (TMS), as shown in Figure S7. ^{1}H NMR spectrum of potassium phenolate (Figure S7a) (DMSO-d_6 with 0.05% v/v TMS, 400 MHz): δ = 6.94 (4Hb", m, J = 9 Hz), 6.61 (4Ha", m, J = 9 Hz), 1.52 (6Hc", s). ^{1}H NMR spectrum of bisphenol A (Figure S7b) (DMSO-d_6 with 0.05% v/v TMS, 400 MHz): δ = 9.13 (1Hd, s), 6.98 (4Hb, m, J = 9 Hz), 6.63 (4Ha, m, J = 9 Hz), 1.53 (6Hc, s). Upon deprotonation of the phenol group by the potassium carbonate, the peak from the phenol group vanished. This was indicative of the successful reaction between bisphenol A and potassium carbonate, and suggested complete conversion of bisphenol A into potassium phenolate.

^{19}F NMR spectra for DFDPS/K^+PhO^- complexes at varying molar ratios were collected. The chemical shift of fluorine shifted upward for DFDPS/K^+PhO^- mixtures relative to DFDPS (Figure S8a) as the ratio of DFDPS:K^+PhO^- increased in the order of 1:0.5, 1:1, 1:1.5, 1:2, 1:2.5 (Figure S8b~f). This can be rationalized by a combination of the effects from electron density changes and paramagnetic contributions,[1] which is the subject of future investigations.

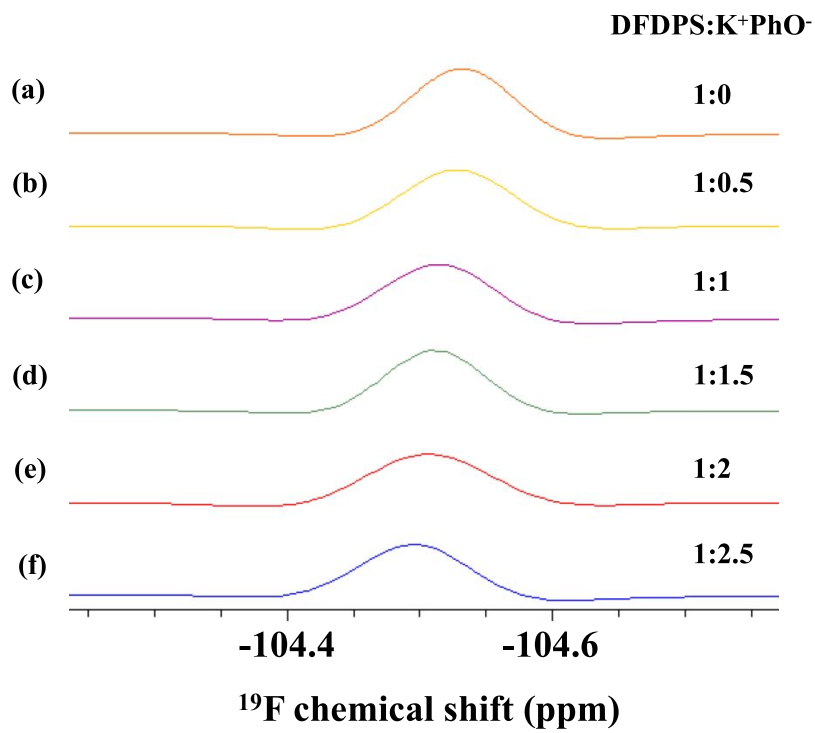

Figure S8. ^{19}F-NMR spectra (DMSO-d_6, 400 MHz) of DFDPS/K^+PhO^- homogenous mixture at room temperature with stoichiometric ratio of (a) 1:0, (b) 1:0.5, (c) 1:1.0, (d) 1:1.5, (e) 1:2.0, (f) 1:2.5, respectively.

Table S1. DFT calculations of the charge states and bond lengths of the related atoms upon complexation of DFDPS with Na^+PhO^- in various stoichiometric ratios.

<table>
<tr><td>F:Na⁺ ratio</td><td>1:0</td><td>1:1</td><td colspan="2">1:2</td></tr>
<tr><td>F</td><td>-0.69 e⁻</td><td>-0.70 e⁻</td><td colspan="2">-0.71 e⁻</td></tr>
<tr><td>Na⁺-1</td><td>N/A</td><td>+0.92 e⁻</td><td colspan="2">+0.93 e⁻</td></tr>
<tr><td>Na⁺-2</td><td>N/A</td><td>N/A</td><td colspan="2">+0.90e⁻</td></tr>
<tr><td rowspan="2">F•••Na⁺</td><td rowspan="2">N/A</td><td rowspan="2">2.26 Å</td><td>F•••Na⁺-1</td><td>2.30 Å</td></tr>
<tr><td>F•••Na⁺-2</td><td>2.69 Å</td></tr>
</table>

NOTE: Charges calculated in VASP using a 550 eV cut off energy at the GAMESS geometries, and the HSE06 functional

Additional comments related to Figure 5 in the main text: after the C-O and C-F bonds have formed and broken, respectively, the Na^+ cation of the NaX product is still complexed to the Ar-O-Ph molecule. It is uphill in energy by ~40 kJ/mol to break this complex for structures considered. If a second NaB is present, i.e. in the three-body case, a second de-coupling reaction must occur to from the final NaF (143 kJ/mol) or NaCl (125 kJ/mol) from NaX•••NaB (i.e., state 3 to 4 to 5 for the three-body mechanism and state 3 to 5 for the two-body mechanism). The strong complexation between NaX and NaB suggests that until NaX crystallizes and forms a solid, it acts to bind and thus trap NaB reactants.

1. References Cited

(1) Dahanayake, J. N.; Kasireddy, C.; Karnes, J. P.; Verma, R.; Steinert, R. M.; Hildebrandt, D.; Hull, O. A.; Ellis, J. M.; Mitchell-Koch, K. R. Progress in Our Understanding of 19F Chemical Shifts. In *Annual Reports on NMR Spectroscopy*; 2018. https://doi.org/10.1016/bs.arnmr.2017.08.002.